ANALYSIS OF MIST/AIR FILM COOLING PERFORMANCE OF TRENCHED HOLES WITH SHAPED LIPS

by

Runsheng ZHANG[a], Leping ZHOU[a,b*], Shaohua HAN[a], Jiangjiang XING[a], Yuanyuan SONG[a], Li LI[a,b], Hui ZHANG[a,b], and Xiaoze DU[a,b]

[a] School of Energy, Power and Mechanical Engineering,
North China Electric Power University, Beijing, China
[b] Key Laboratory of Power Station Energy Transfer Conversion and System
(North China Electric Power University), Ministry of Education, Beijing, China

Original scientific paper
https://doi.org/10.2298/TSCI220801185Z

Mist-assisted film cooling has exhibited great potential for efficient cooling of a turbine blade. Trench structures can significantly affect the film cooling performance of air, while their impact on the adhesion characteristics of the droplets and thus the mist-assisted film cooling performance is unclear. This work highlights the combination of these two aspects by exploring the improvement of the mist-assisted film cooling performance for trenched holes with shaped lips using 3-D computations. The results show that the upper lip structure plays a significant role in the adiabatic film cooling effectiveness, whereas the lower lip structure has little effect on it. It is found that the effect of upper lip structure on the adiabatic film cooling effectiveness increases with increasing blowing ratio. The Coanda effect makes the droplets more attached to the wall of the upper fillet lip structure and upper bevel lip structure. Meanwhile, the concentration of mist and the diameter of droplets are crucial for significantly improving the adiabatic film cooling effectiveness. In general, better adiabatic film cooling effectiveness values are observed for both 10 μm diameter droplets at a specified concentration of mist and larger concentration of mist at a specified droplet size. This work proposes a novel and efficient means of enhancing the cooling performance using mist/air mixture and trenched holes with shaped lips.

Key words: *film cooling effectiveness, trench, lips, blowing ratio, mist*

Introduction

The gas turbine is an advanced and clean energy conversion device, which is widely used in various fields, such as energy, transportation, military*, etc.* One of the most effective ways to improve the effectiveness of gas turbine is to increase the inlet temperature. However, due to the slow progress in the development of superalloy materials, the high temperature thermal resistance of the vane is limited. The application of advanced film cooling technology helps to increase the heat resistance limit of vanes. As is known to all, film cooling technology avoids direct contact of hot gas with the turbine blade surface by injecting a layer of coolant along the surface [1]. Compared to the fan-shaped hole [2], *Y*-shaped hole [3], counter-inclined hole [4], and round-to-slot hole [5], the trenched hole can be formed by cutting the thermal barrier coating, thus avoiding the complicated machining of the blade metal. For the transverse trench,

* Corresponding author, e-mail: lpzhou@ncepu.edu.cn

the depth and width of it have a significant impact on the film cooling effectiveness (FCE) [6]. The experimental results showed that, compared with a individual jet, trenching holes in the trench cannot only reduce the jet momentum at the outlet, but also improve the spanwise coverage of the jet. Furthermore, they also noted that the best film cooling performance was exhibited when the trench depth was 0.75*D*. Li *et al.* [7] compared both experimentally and computationally the FCE of three compound angles (0°, 45°, and 90°) of the cooling hole and found that it performed best at 45°. Besides the transverse trench, some new trench structures have been proposed in recent years. Because of the Coanda effect, the FCE of the fillet trench can be improved to a certain extent compared to the transverse trench [8]. Through numerical simulation, Zhang *et al.* [9] found that the trench lip structure has an important influence on the FCE. It was found that the upper lip structures had a greater effect on FCE than the lower lip structures at the blow ratios studied.

Many previous works show that mixing mist into the cooling fluid can effectively improve the FCE. For example, Wang *et al.* [10] used numerical simulation study the effect of film hole blockage on cooling effectiveness in the case of mist cooling. It was found that the blockage in the hole will reduce the lateral FCE. It was also pointed out that when the blowing ratio is 0.6, the cooling performance can be improved by about 10% by adding 1% mist. Tian *et al.* [11] proposed a new film hole structure. Through simulations, they found that the new structure has a wider coverage area than traditional cylindrical air film holes. In addition, for the mist cooling, it can also significantly improve the cooling performance. Guo *et al.* [12-14] and Gao *et al.* [15] investigated the heat transfer process of mist/steam cooling superheated wall through experiments, and found that in the straight pipe test section, when 5% mist was mixed in the air, 100% of the average enhancement can be obtained, and the local heat transfer strengthening enhancement can reach up to 200%. In the 180° elbow test section, it can be found that the heat transfer performance is significantly improved when fine droplets are added to the air-flow. Then for the ribbed channel, the addition of droplets reduces the average temperature of its inner wall by 71.2 K. Li *et al.* [16] also numerically simulated the effect of mixing mist in the coolant on FCE. They showed blending 2% mist can provide 30-50% enhancement. They further set up the model with different settings and compared their effects and found that the effect of turbulent dispersion on the cooling of the mist/film is dominant, followed by the thermophoretic force and then the Brownian force and Saffman lift [17]. Their computations also showed blending 2-10% mist can reduce the heat transfer coefficient and provide more uniform wall surface temperature under actual working conditions (15 atm and 1561 K) [18]. Barrow *et al.* [19] studied the relationship between the airborne lifetime and the maximum time of a droplet in a given environment, based on the settling time of a free-falling droplet. Dhanasekaran *et al.* [20, 21] studied the influence of droplet parameters on the cooling performance under experimental conditions and actual gas turbine operating conditions by experiments and simulations, respectively. The results showed that the mist/steam cooling technology can achieve an average cooling enhancement of 50-100%. Abdelmaksoud *et al.* [22] numerically studied the effect of adding mist droplets on the FCE of gas turbine vanes using a conjugate heat transfer method. The results show that using a uniform droplet size distribution at the first 40% of the vane height provides significantly better cooling enhancement than a non-uniform droplet size distribution. Rao *et al.* [23] numerically studied the effect of droplet parameters on the FCE of a cylindrical hole using a 2-D model. They showed that the FCE increases with decreasing droplet diameter when the mass-flow rate of dry air is specified, while it increases with the increase in the relative humidity of air. Further, conducted an experimental study of mist cooling on a flat plate and found that when 2.1% of the mist is

added to the air, it can increase the FCE of the flat plate by 26% and can improve the coverage in the flow and span directions. Handique *et al.* [24] performed numerical analysis of flat film cooling of air and mist injection from a slot, and investigated the effects of soot deposition and cooling slot erosion in the presence of an upstream ramp. Pabbisetty *et al.* [25] experimentally investigated the effect of blowing ratio on FCE and suggested that cooling air can be mixed with an appropriate amount of water mist to enhance FCE. Nirmalan *et al.* [26] showed the mist cooling effect on blades through cascade experiments, which demonstrated that the mist can produce up to 0.9 cooling effectiveness in some areas of the blade surface. Zhang *et al.* [27] numerically simulated the effect of mist/air on the cooling structure of a double-walled vane. The results showed that when the cooling medium is mist/air, the cooling performance of the double-wall structure is significantly improved. Sozbir *et al.* [28] studied the heat transfer mechanism of water mist impingement on high temperature metal surface. They found that the heat transfer coefficient of water mist impingement cooling has a similar trend to that of air and the heat transfer is significantly enhanced by adding a small amount of water to the air.

From the aforementioned literature survey, it is clear that adding mist to the coolant air can improve the FCE of gas turbine vanes. The trenched holes can also effectively improve the FCE compared to the cylindrical hole. However, whether the trenched holes with mist added to the coolant air can further improve the FCE remains unclear, which is worthy of study. Our prior work investigated the influence of trench and lip using air as coolant [9]. It was found that the impact of the upper lip is more apparent than the lower lip structures at different blowing ratios. In the present work, the FCE of trenched holes with different lips using air/mist coolant and the effect of mist concentration and droplet diameter on the FCE will be systematically studied.

Simulation method

Modelling

The FCE of the hole structures, see also [9], are calculated in this simulation. First, a cylindrical film hole (Case 1) is used for comparison. Then, eight different hole structures are designed, with fillets and bevels being permutated at the upper and/or bottom of a transverse trench (Case 2). Details of the permutation design in these structures (Cases 3-9) are schematically shown in fig. 1. For the double-curvature (DC) trench (Case 6), the right wall composes of two quarter circles, and its edge is set as the origin (X/D = 0). The parameters of the hole structures are presented in tab. 1.

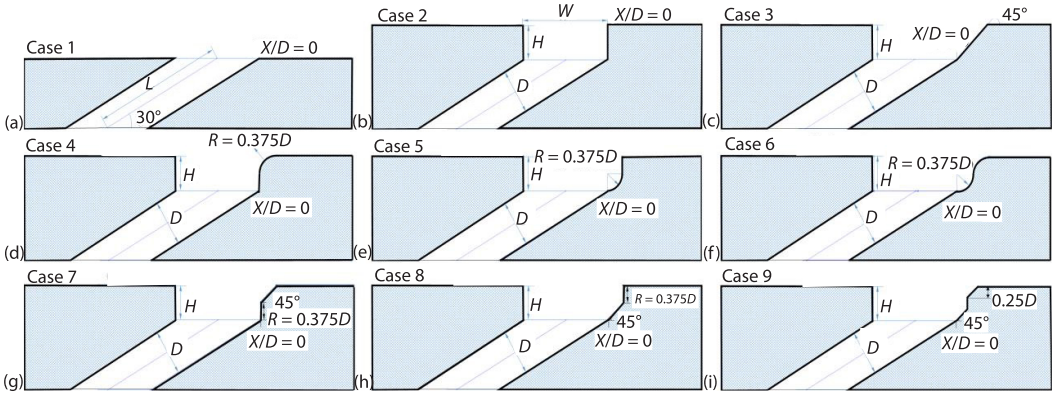

Figure 1. Schematic diagram of film cooling holes

Table 1. Parameters of hole structures

Parameters	Value
D	12.7
W/D	2
H/D	0.75
S/D	3
L/D (without trench)	2.25

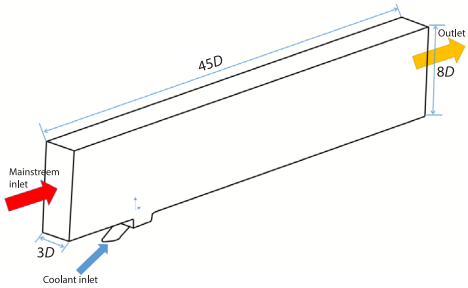

Figure 2. Geometry of numerical model

Figure 2 schematically shows the geometry used for the calculation. Table 2 lists the boundary conditions. The blowing ratio, M, which is determined by the velocities momentum of mainstream and inlet coolant, is 0.5, 1.0, or 1.5. The initial temperature and velocities of the droplets are the same as the inlet air. The insulated and non-slip boundary conditions of the wall are set to calculate the FCE. The outlet pressure is kept at 1 atm. Since multiple film cooling holes are distributed side by side in the actual vane and the jet ejecting from a single film cooling hole is affected by the adjacent jets, the sidewalls are set to be the transition period boundary condition. The computational software FLUENT in ANSYS 19.2 is used in numerical calculations. The standard model of k-ε turbulence with augmented treatment at the wall is employed because of its robustness [16]. The mainstream Reynolds number based on the inlet hydraulic diameter and the inlet velocity is about 21174 in this study.

Table 2. Boundary conditions

Boundary conditions	Parameters	Values
Coolant		Air/mist
Inlet temperature of mainstream [K]	T_g	400
Inlet velocity of mainstream [ms^{-1}]	U_g	10
Inlet temperature of coolant [K]	T_c	300
Mist concentrations [%]	m	1, 2, 10
Diameters of droplets [μm]	d	1, 10, 20

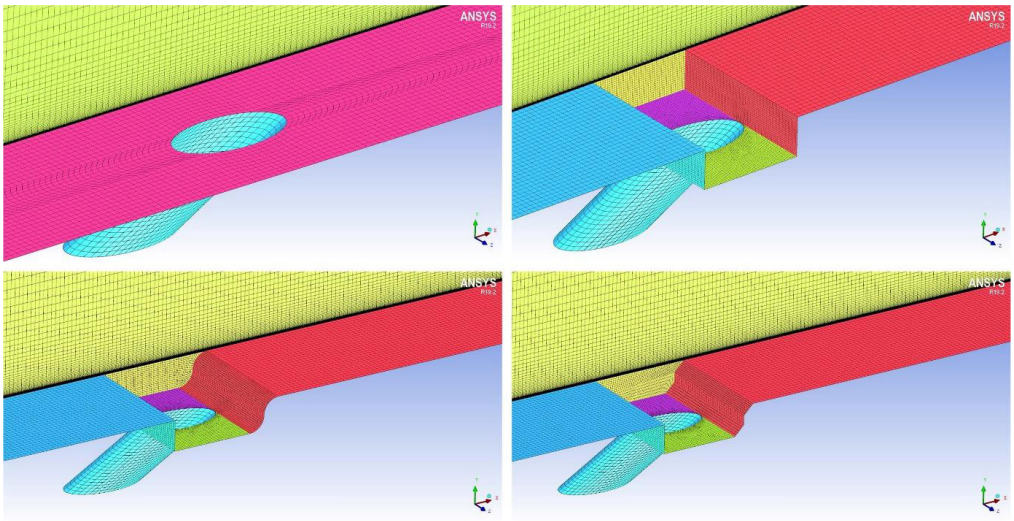

Figure 3. Grids generated in computing domain

Governing equations

The equations of the continuous phase, discrete phase, and stochastic particle tracking in this paper can be referred to in our previous work [16].

Verification of grid independence

Figure 3 shows the grids generated in the computing domain. The structured grids and the unstructured grids (trench area) for Cases 1, 2, 6, and 9 are generated in the entire computing domain. The grid $y+$ is less than 1.0 to meet the requirement of calculation accuracy. Figure 4 compares the calculations of different grid numbers, which shows almost identical distributions of η. Therefore, 1.13 million grids will be used in the following simulations of this work.

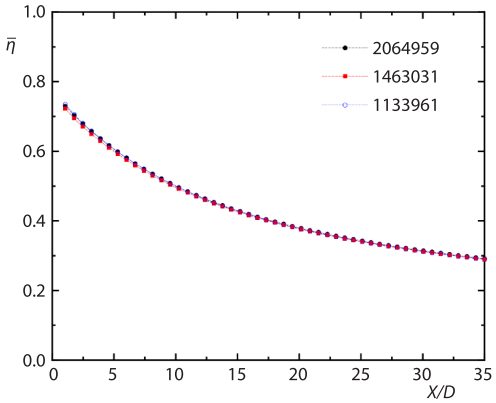

Figure 4. Grid independence verification

Verification of the numerical method

The simulations of FCE are validated against the experimental work by Guo *et al.* [12]. Figure 5(a) shows the obtained FCE of coolant air with a mist concentration of 7.14% in their experiment. It can be found that the present simulations show good agreement with the experimental data. The numerical simulation method is verified by further comparing an experimental study of temperature distribution when the coolant air contains 5.7% of mist [12]. As shown in fig. 5(b), the simulation results are basically consistent with the experimental data. It should be emphasized that DT is the diameter of the horizontal tube, and for the sake of comparison, the Fahrenheit temperature used in the experimental study by Dhanasekaran *et al.* [21] is converted to thermodynamic temperature here.

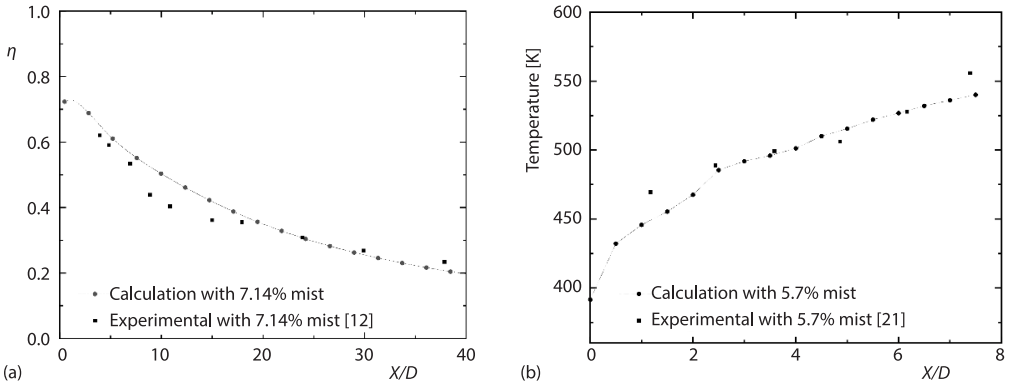

Figure 5. Comparison between present simulation and experimental work

Results and discussion

Effect of blowing ratio on FCE

In this subsection, the diameter of the droplets is 10 μm and the mist concentration is 2%. First, the area-average FCE are compared, as shown in fig. 6. A region on the plate (1*D*-35*D* along *X*-direction, and –1.5*D*-1.5*D* along *Y*-direction) is used for the calculations.

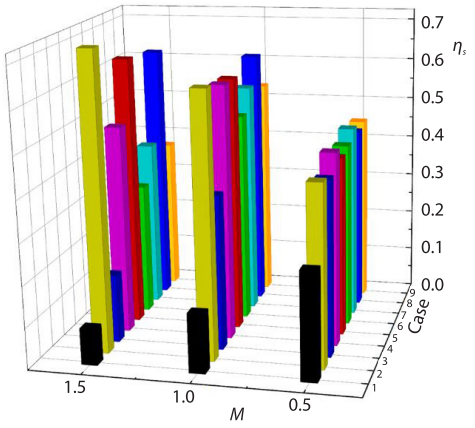

Figure 6. Area-average FCE at different blowing ratios

The value of Case 1 is lower than those of Cases 2-9 for M = 0.5, 1.0, and 1.5. Figure 7 also shows that the value of Cases 1 and 3 decreases with an increasing blowing ratio. This is contrary to Case 2, which has an increasing value with the blowing ratio. When M = 0.5, the FCE differences for Cases 2-9 are not obvious; as M increases, the differences become apparent. This shows that from 0.5 to 1.5, the greater the blowing ratio, the greater the influence of the lip structure on the FCE. Under all three blowing ratio conditions, the FCE of Case 3 among Cases 2-9 is the lowest. This is because its lip structure severely weakens the blocking effect of the trench on the coolant flow, making it difficult for the coolant flow to fit the cooling wall when its momentum is too large. When M = 0.5, the FCE of Cases 4-9 are higher than that of Case 2, showing that the lip structure favors the improvement of FCE at low blowing ratios. When M = 1.5, the FCE of Cases 2, 5, and 8 are considerably higher than other cases, showing that when the blowing ratio is high, a vertical upper lip structure favors the FCE improvement.

To understand how the effectiveness varies along the X-direction for all the cases, the span-wise average FCE are calculated. It can be observed from figs. 6 and 7 that the span-wise average and area-average FCE show consistent tendencies. When M = 0.5, the FCE of Cases 2-9 gradually decrease along the X-direction. When M = 1.5, the span-wise average FCE of Cases 2, 5, and 8 first increase and then decrease along the X-direction. Correspondingly, the span-wise average FCE of other trench holes first decrease and then slowly increase along the X-direction. This shows that the coolant leaves the outlet of the hole and then is pressed by the mainstream at the wall. By comparing the span-wise average FCE of Cases 2, 4, and 5 (and Cases 2, 7, and 8), it can be seen that the lower trench corner has a negligible impact on the FCE of the lip, while the upper lip dominates the performance.

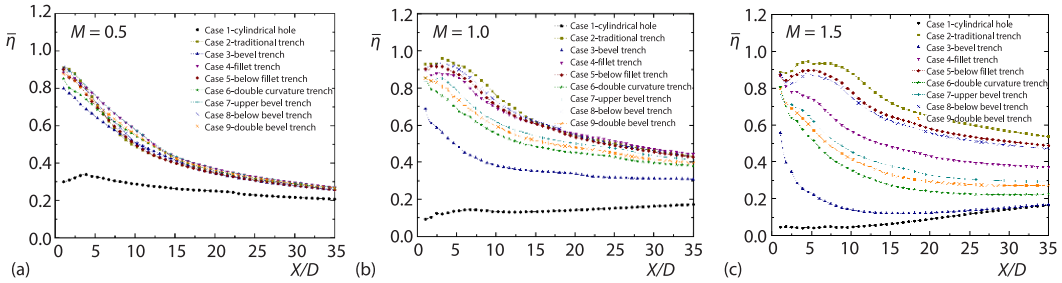

Figure 7. Span-wise average FCE at different blowing ratios

Figures 8-10 show the droplet trajectories along the X-direction for 10 μm droplets with 2% of mist at M = 0.5, 1.0, and 1.5, with both 3-D and 2-D views. It can be seen from them that the trenches have an obvious blocking effect on the droplets coming out of the film cooling holes along the mainstream direction, and therefore, making the droplets expand in the span-wise direction. From the 2-D view, we can see that when the blowing ratio is 0.5, the droplets fit well to the wall. As M increases, the droplets gradually depart from the wall. When

the blowing ratio is 1.5, the trenched holes with fillet or bevel upper lip structures (Cases 3, 4, 6, 7, and 9) and the trenched holes without upper lip structures present the droplet trajectory closer to the cooling wall. This is owing to the Coanda effect [29], which describes how a jet follows the contour of an adjoining boundary even if they are leaving from the axis of the jet. This effect is usually caused by a pressure gradient along the normal direction of the curved streamline, where the pressure gradient is proportional to $\rho V^2/r$ (r is the curvature radius of the surface). Under the influence of this effect, the flow emanating from the film hole is forced to adhere to the surface. Subsequently, a slight increase in viscous drag on the coolant, combined with fluid entrainment between the coolant and the surface, makes the coolant more inclined to move towards the surface [11]. Induced by the pressure gradient in the normal direction of the streamline [30], the coolant flow from the trenched holes with upper lip structures fits more closely to the wall.

Our previous study [11] has demonstrated the influence of the trench shape on kidney vortex by comparing the velocity vector and the vortex structure. So, we do not repeat it in this work. The FCE decreases significantly when the droplets are added to the cooling air. This is mainly because of the evaporation and heat absorption of the droplets, rather than the change of the kidney vortex.

Influences of mist concentration and droplet size on FCE

As the fillet trench can full use the Coanda effect by the more closely fit of droplets to the wall, and there is also a lack of knowledge of the mist-assisted FCE for fillet trench,

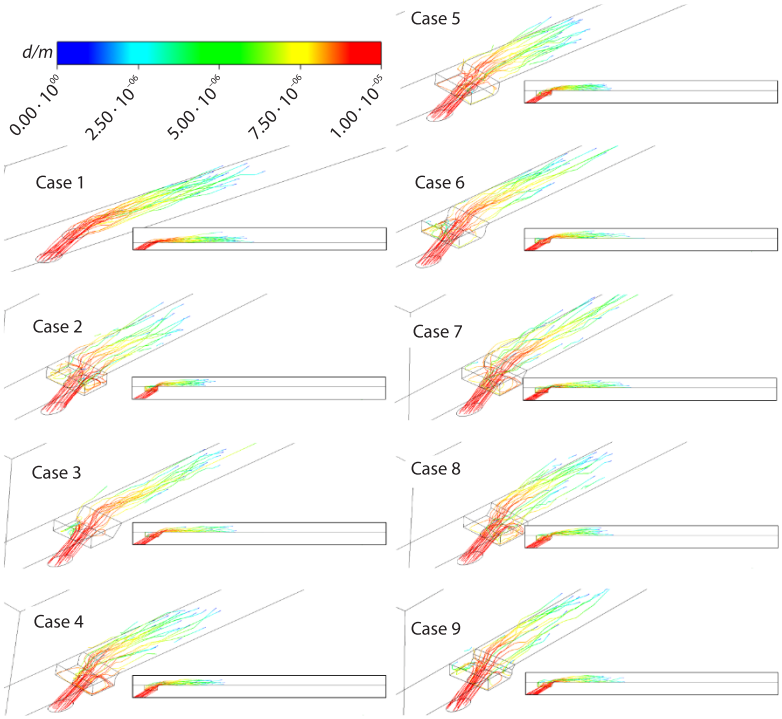

Figure 8. Droplet trajectories along the *X*-direction for 10 μm droplets with a concentration of 2% at $M = 0.5$

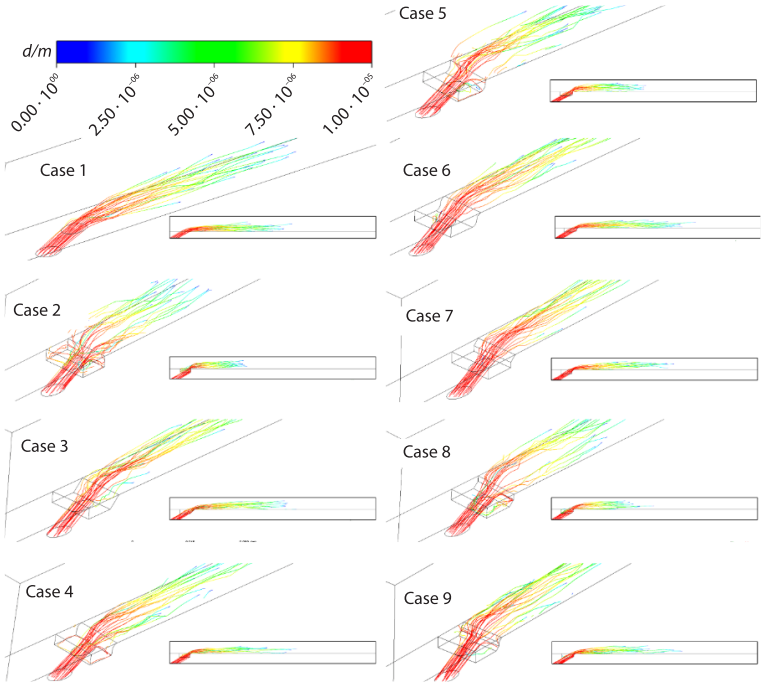

Figure 9. Droplet trajectories along the *X*-direction for 10 μm droplets with a concentration of 2% at *M* = 1.0

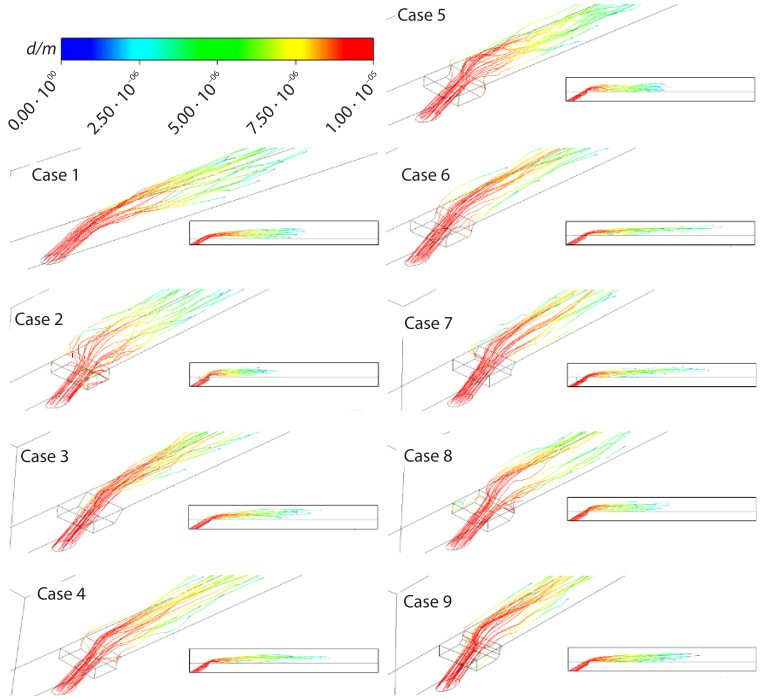

Figure 10. Droplet trajectories along the *X*-direction for 10 μm droplets with a concentration of 2% at *M* = 1.5

Case 4 is selected to study the effect of mist concentration and droplet diameter on FCE in this subsection. The span-wise average FCE of Case 4 for different mist concentrations (2%, 5%, and 10%) and droplet diameters (1 μm, 10 μm, and 20 μm) at $M = 1.0$ is shown in fig. 11. For $X/D > 20$, the FCE of Case 4 is divided into four groups according to the mist concentration (0, 2%, 5%, and 10%). Between 0 to 10%, the FCE of Case 4 increases with increasing concentration. At the concentration of 2%, the FCE with droplet diameters of 1 μm and 10 μm are very close and higher than those with a droplet diameter of 20 μm. At the concentration of 5%, the FCE has the highest value, with a droplet diameter of 10 μm, followed by 1 μm and 20 μm droplets. At the concentration of 10%, the FCE at the droplet diameter of 10 μm is higher than those at the other two diameters. Under different concentration conditions, the order of FCE with the change of droplet diameter is not the same, but it can be still seen that the FCE at the droplet diameter of 10 μm has the highest value. Compared to coolant air, the percentage enhancement of the FCE for $d = 10$ μm and 10% of mist is 30-207%.

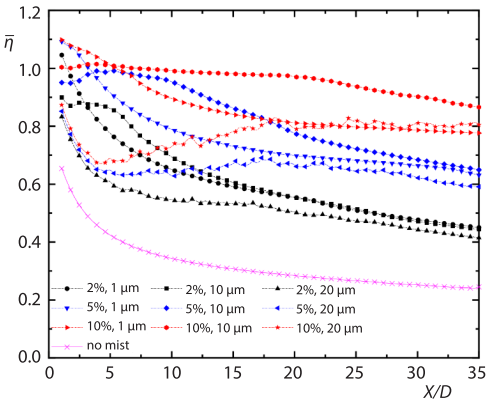

Figure 11. Span-wise average FCE of Case 4 for different mist concentrations and droplet diameters at $M = 1.0$

The contours of FCE of the fillet trench (Case 4) for different mist concentrations (2%, 5%, and 10%) and droplet diameters (1 μm, 10 μm, and 20 μm) at $M = 1.0$ are shown in fig. 12 to examine how the film covers the surface. By comparing the areas with high FCE ($\eta > 0.75$), it can draw a similar conclusion the previous subsection that the FCE of Case 4 increases with increasing concentration and the FCE at the droplet diameter of 10 μm has the highest value. When the diameter of the droplet is 20 μm, there are more areas with high FCE, because the droplets fall on the cooling wall and evaporate.

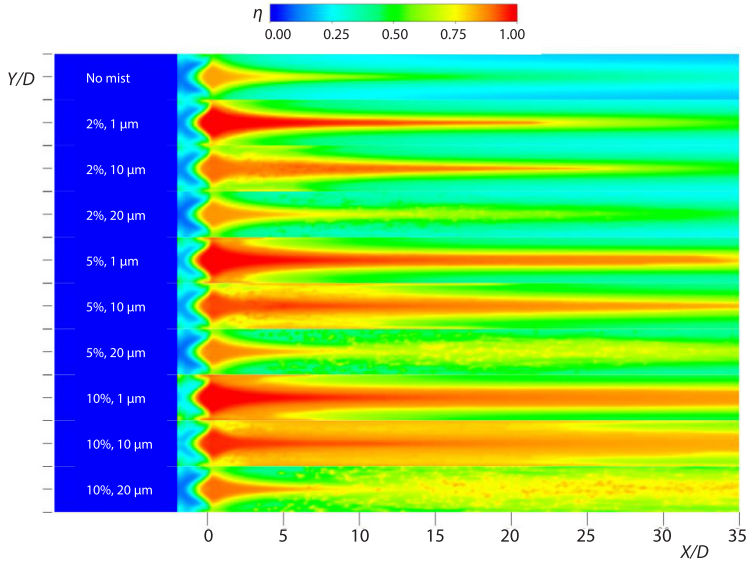

Figure 12. Distribution of FCE of the fillet trench (Case 4) for different mist concentrations and droplet diameters at $M = 1.0$

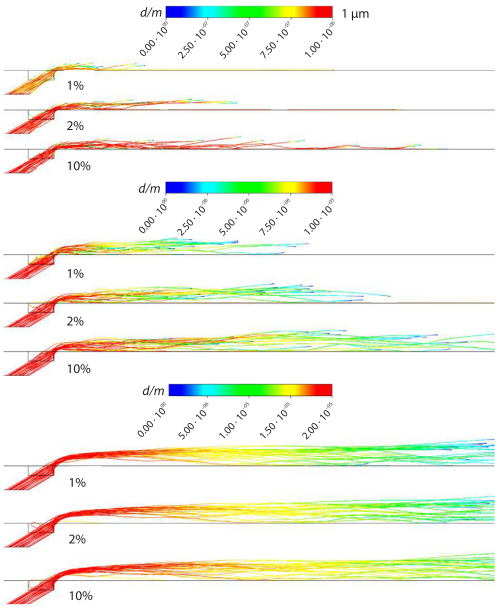

Figure 13. Droplet trajectories along the *X*-direction of the fillet trench (Case 4) for different mist concentrations and droplet diameters at *M* = 1.0

Figure 13 shows the trajectories of droplets obtained from a method of stochastic tracking, which considers the dispersion of turbulence. As expected, the larger the diameter of the droplet, the longer the distance reached before they completely evaporate. It can also be found that the greater the concentration, the farther the droplets reach before they disappear. This is because, with the same droplet diameter, a higher concentration results in less heating of a single droplet, and hence it will reach a longer distance before completely evaporating.

Conclusion

A 3-D computational investigation on the mist-assisted film cooling is implemented for several trenched holes. Mist is mixed in the air, and the effects of trench lip structure, blowing ratio, mist fraction, and droplet size are observed. The major conclusions are summarized as follows. The upper lip structure is critical for determining the FCE, whereas the lower lip structure has little effect on it. In addition, the effect of upper lip structure on the FCE increases with increasing blowing ratio. The Coanda effect makes the droplets of the upper fillet lip structure and upper bevel lip structure more attached to the wall. The mist fraction and droplet size are two key parameters that significantly affect the FCE. In general, better FCE values are obtained for 10 μm diameter droplet at a specified mist fraction and higher mist fraction at a specified droplet size

Acknowledgment

The authors are grateful for the financial support from the National Major Science and Technology Projects of China (No. 2017-III-0003-0027).

References

[1] Bogard, D. G., *et al.*, Gas Turbine Film Cooling, *Journal of Propulsion and Power*, *22* (2006), 2, pp. 249-270
[2] Song, Y. J., *et al*., Effects of Trench Configuration on the Film Cooling Effectiveness of a Fan-Shaped Hole, *International Journal of Heat and Mass Transfer*, *178* (2021), 121655
[3] Li, L., *et al*., Experimental Investigation on Effects of Cross-Flow Reynolds Number and Blowing Ratios to Film Cooling Performance of the Y-Shaped Hole, *International Journal of Heat and Mass Transfer*, *179* (2021), 121682
[4] Zhang, B. L., *et al*., Experimental Study on Film Cooling and Heat Transfer Characteristics of a Twisted Vane with Staggered Counter-Inclined Film-Hole and Laid-Back-Shaped-Hole, *International Journal of Heat and Mass Transfer*, *176* (2021), 121377
[5] Zhu, X. D., *et al*., Numerical Assessment of Round-to-Slot Film Cooling Performances on a Turbine Blade under Engine Representative Conditions, *International Communications in Heat and Mass Transfer, 100* (2019), Jan., pp. 98-110
[6] Lu, Y., *et al.*, Effect of Trench width and Depth on Film Cooling From Cylindrical Holes Embedded in Trenches, *Journal of Turbomachinery*, *131* (2009), 1, 011003

[7] Li, J., *et al*., Film Cooling Performance of the Embedded Holes in Trenches with Compound Angles, *Proceedings*, Turbo Expo: Power for Land, Sea, and Air, Glasgow, UK, 2010, Vol. 43994, pp. 1415-1424
[8] Idowu Oguntade, H., *et al.*, Improved Trench Cilm cooling with Shaped Trench Outlets, *Journal of Turbomachinery*, *135* (2013), 2, 021009
[9] Zhang, R., *et al*., Numerical Evaluation of Film Cooling Performance of Transverse Trenched Holes with Shaped Lips, *International Communications in Heat and Mass Transfer*, *125* (2021), 105326
[10] Wang, J., *et al*., Effect of Spherical Blockage Configurations on Film Cooling, *Thermal Science*, *22* (2018), 5, pp. 1933-1942
[11] Tian, K., *et al*., Effect of Combined Hole Configuration on Film Cooling with and Without Mist Injection, *Thermal Science*, *22* (2018), 5, pp. 1923-1931
[12] Guo, T., *et al*., Mist/Steam Cooling in a Heated Horizontal Tube – Part 1: Experimental System, *Journal of Turbomachinery*, *122* (2000), 2, pp. 360-365
[13] Guo, T., *et al*., Mist/Steam Cooling in a Heated Horizontal Tube – Part 2: Results and Modelling, *Journal of Turbomachinery*, *122* (2000), 2, pp. 366-374
[14] Guo, T., *et al*., Mist/Steam Cooling in a 180-Degree Tube Bend, *ASME Journal of Heat Transfer*, *122* (2000), 4, pp. 749-756
[15] Gao, T., *et al.*, Numerical Prediction on Mist/Steam Cooling in a Square Ribbed Channel at Real Gas Turbine Operational Conditions, *International Journal of Heat and Mass Transfer*, *108* (2017), May, pp. 1089-1102
[16] Li, X., *et al*., Simulation of Film Cooling Enhancement with Mist Injection, *ASME Journal of Heat Transfer*, *128* (2006), 6, pp. 509-519
[17] Li, X., *et al*., Effects of Various Modelling Schemes on Mist Film Cooling Simulation, *ASME Journal of Heat Transfer*, *129* (2007), 4, pp. 472-482
[18] Li, X., *et al*., Two-Phase Flow Simulation of Mist Film Cooling on Turbine Blades with Conjugate Internal Cooling, *ASME Journal of Heat Transfer*, *130* (2008), 10, 102901
[19] Barrow, H., *et al.*, Droplet Evaporation with Reference to the Effectiveness of Water-Mist Cooling, *Applied Energy*, *84* (2007), 4, pp. 404-412
[20] Dhanasekaran, T. S., *et al.*, Simulation of Mist Film Cooling on Rotating Gas Turbine Blades, *Journal of Heat Transfer*, *134* (2012), 1, 011501
[21] Dhanasekaran, T. S., *et al*., Validation of Mist/Steam Cooling CFD Model in a Horizontal Tube, *Proceedings*, Heat Transfer Summer Conference, Jacksonville, Fla., USA, 2009, pp. 611-624
[22] Abdelmaksoud, R., *et al*., Simulation of Air/Mist Cooling in a Conjugate, 3-D Gas Turbine Vane with Internal Passage and External Film Cooling, *International Journal of Heat and Mass Transfer*, *160* (2020), 120197
[23] Rao, P. M., *et al.*, A Computational Study of Mist Assisted Film Cooling, *International Communications in Heat and Mass Transfer*, *95* (2018), July, pp. 33-41
[24] Handique, J., *et al*., Effects of Soot Deposition and Slot Erosion on the Mist Film-Cooling of a Flat Plate in the Presence of Upstream Ramp, *Thermal Science and Engineering Progress*, *22* (2021), 100784
[25] Pabbisetty, M. R., *et al*., Effect of Blowing Ratio on Mist-Assisted Air Film Cooling of a Flat Plate: An Experimental Study, *Journal of Thermal Science and Engineering Applications*, *13* (2021), 3, 031016
[26] Nirmalan, N. V., *et al*., An Experimental Study of Turbine Vane Heat Transfer with Water-Air Cooling, *Journal of Turbomachinery*, *120* (1998), 1, pp. 50-60
[27] Zhang, R., *et al*., Impingement/Film Cooling of C3X Vane with Double-Wall Cooling Structure Using Air/Mist Mixture, *International Journal of Heat and Mass Transfer*, *188* (2022), 122594
[28] Sozbir, N., *et al*., Heat Transfer of Impacting Water Mist on High Temperature Metal Surfaces, *Journal of Heat Transfer*, *125* (2003), 1, pp. 70-74
[29] Panitz, T., *et al.*, Flow Attachment to Solid Surfaces: The Coanda Efect, *AIChE Journal*, *18* (1972), 1, pp. 51-57
[30] Houghton, E. L., Carpenter, P. W., *Aerodynamics for Engineering Students,* Elsevier, Amsterdam, The Netherlands, 2003

Paper submitted: August 8, 2022
Paper revised: October 7, 2022
Paper accepted: October 19, 2022